International Journal of Mechanical Sciences 107 (2016) 188–200

Contents lists available at ScienceDirect

International Journal of Mechanical Sciences

journal homepage: www.elsevier.com/locate/ijmecsci

Numerical simulations of the fatigue damage evolution at a fastener hole treated by cold expansion or with interference fit pin

Ying Sun, Weiping Hu *, Fei Shen, Qingchun Meng, Yuanming Xu

School of Aeronautics Science and Engineering, Beihang University, Room D604, New Main Building, 37th Xueyuan Road, Beijing 100191, China

ARTICLE INFO

Article history:
Received 10 August 2015
Received in revised form
7 December 2015
Accepted 12 January 2016
Available online 18 January 2016

Keywords:
Cold expansion
Interference fit
Fatigue damage
Continuum damage mechanics
Finite element

ABSTRACT

Numerical simulations of the fatigue damage evolution at a hole in a plate treated by cold expansion or with interference fit pin is performed based on continuum damage mechanics and the finite element method. The damage-coupled Chaboche plasticity constitutive model is used to model the mechanical behavior of material. Plastic-strain-based and stress-based equations are used to calculate damage accumulation. The process of the hole cold expansion or pin interference fit and the subsequent fatigue damage evolution are simulated. The predicted results agree well with the experimental data available in the literature. Result shows that the beneficial effect of cold expansion and interference fit on the fatigue life improvement of a fastener hole is not only due to the reduction in maximum stress or stress amplitude, but also to the change in the fatigue damage evolution at the critical location.

1. Introduction

For many mechanical joints subjected to cyclic loads, fatigue cracks typically develop at fastener hole stress concentrations. In order to increase fatigue resistance of mechanical joints such as rivet and bolt joints, hole cold expansion or interference fit fasteners are widely used in aeronautical industry. In the cold expansion process, a significant amount of plastic deformation is produced around the hole by pulling an oversized tapered mandrel through the fastener hole. This process creates compressive residual stresses around the hole due to the recovery of the elastic deformation in the material. The compressive residual stresses reduce the maximum tensile stresses at critical locations when the component is subjected to tensile cyclic loading [1]. In the interference fit process, an oversized pin or bolt is inserted into the fastener hole during component assembly. This process creates mainly tensile residual stresses around the hole due to the hole being expanded by the oversized pin or bolt. Although the tensile residual stresses increase the mean stress when subjected to cyclic loading, the stress amplitude is significantly reduced due to the 'support effect' of the pin or bolt [2] and leads to fatigue life improvement. Either cold expansion or interference fit improves the fatigue resistance of the fastener hole by changing the stress and strain distributions around the hole.

Studies [3,4] has demonstrated that the cold expansion can improve the fatigue life of a fastener hole by a factor of 3–10. The beneficial effect of cold expansion is attributed to the compressive residual stress, which has the effect of extending both the crack nucleation and crack propagation periods by large proportions [1]. Experimental and finite element methods [5] were used to calculate the residual stress field. It is known that the fatigue striation crack lengths and the crack growth rates of cold expanded specimens are smaller than for those with untreated open hole [6–8]. There are scatter studies that have investigated the effect of interference fit on fatigue life of bolted or pinned joints [9–11]. It is supposed that the reduction in stress amplitude is the primary reason for the fatigue life improvement. However, the studies of hole cold expansion and holes with interference fit rely upon experimental tests, and the knowledge for fatigue life improvement is limited to date and the explanations remain largely qualitative [10,12,13]. It is difficult to quantitatively analyze the effects of hole cold expansion or holes with interference fit on the resultant fatigue life improvement.

To estimate the residual stress effect on the fatigue life improvement of a fastener hole, life prediction methods require the inclusion of the analysis of residual stress and strain distributions around the hole. Chakherlou et al. [14,15] used the finite element method combined with different critical plane criteria (e.g., Glinka [16], Smith–Watson–Topper [17], Fatemi-Socie [18], etc.) to estimate the fatigue lives of specimens with cold expanded holes and holes with interference fit fasteners and showed that none of the criteria gave accurate results for all of the specimens tested. Matos et al. [19] used an analytical fracture mechanics

* Corresponding author. Tel.: +86 10 82338489.
E-mail address: huweiping@buaa.edu.cn (W. Hu).

http://dx.doi.org/10.1016/j.ijmecsci.2016.01.015
0020-7403/

approach to assess the effects of cold expansion on the fatigue life of a rivet hole. However, the approach simplified the cold expanded specimen into a 2D problem, and therefore failed to describe the fatigue crack location accurately. To predict the fatigue damage in cold expanded holes and those with interference fit fasteners, the conventional analytical methods only consider the effect of residual stress; plasticity damage and the subsequent fatigue damage evolution is not fully understood. Continuum damage mechanics provide a new method for describing the damage evolution in the material.

Continuum damage mechanics (CDM) [20] introduces a continuous damage variable to describe the degradation of materials. Based on thermodynamic and corresponding damage mechanisms, damage evolution laws combined with damage-coupled elasto-plastic or visco-plastic constitutive models can be used to model the evolution of ductile plastic damage, fatigue, creep and creep-fatigue interaction. The fundamental concepts of CDM can be found in publications by Kachanov [21], Lemaitre [22], as well as Lemaitre and Chaboche [23]. CDM has been widely used in engineering applications and research, which can also be used to simulate complicated mechanical behavior such as ratcheting-fatigue interaction [24] and fretting fatigue [25,26]. For accurate applications and when the coupling between strains and damage is strong, a coupled CDM approach is necessary. The constitutive models need to be implemented within a finite element code, and the damage accumulate cycle by cycle to take account of the material degradation and stress redistributions [27].

In this paper, the continuum damage mechanics approach combined with the finite element method are used to simulate the fatigue damage evolution in a fastener hole treated by cold expansion or with interference fit pin. Firstly, the process of cold expansion or interference fit is simulated to obtain the residual stress and strain field and the plasticity damage in the hole caused by those processes. Then the fatigue damage is simulated with consideration of residual stress, and elasticity and plasticity damage. The damage-coupled Chaboche plasticity constitutive model [23] is used to represent the material behavior, and plastic-strain-based and stress-based equations are used to calculate damage accumulation, which is implemented by a user material subroutine (UMAT in ABAQUS). The critical-plane SWT approach is used for comparison purposes. The performance of the proposed approach is verified by comparison with experimental results available in the literature, and to show to be superior to the SWT approach. The effects of cold expansion and interference fit pin on fatigue damage of a fastener hole are investigated.

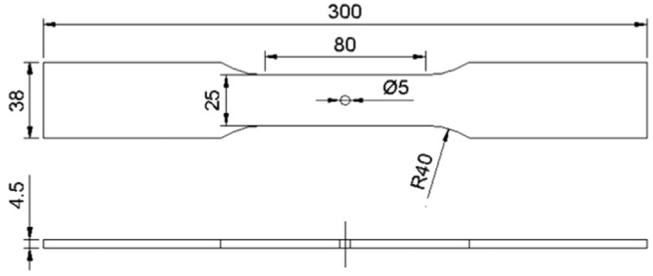

Fig. 1. Dimensions of the open hole specimens (mm) [28].

2. Fatigue experiments

The experiments of specimens with cold expanded hole and holes with interference fit pins performed by Chakherlou et al. [2,28] are simulated in this study. A brief overview of the experiments is presented here.

In the fatigue test of specimens with cold expanded holes [28], two groups of specimens (open hole and cold expanded) made of Al alloy 7075-T6 were tested. Fig. 1 shows the dimensions of the open hole specimen, in which the diameter of the central hole is 5 mm. The hole cold expanded specimen was produced by pulling an oversized tapered pin through the hole. The schematic of the process is shown in Fig. 2(a). The pin was made of En 24 grade steel and has an outer diameter of 5.2 mm, which will be used to produce a cold expansion of 4%. The dimensions of the pin are shown in Fig. 2(b). Fatigue tests were performed under the pulsating cyclic loading (loading ratio is zero). The applied cyclic loading P_{max} and the maximum remote stress in the cross-sectional area are shown in Table 1, and the fatigue test results are shown in Fig. 4(a).

To investigate the effect of pin interference fit on fastener hole fatigue life improvement, four groups of interference fitted specimens and one group of open hole specimens were tested in the literature [2]. The pin interference fitted specimen (Fig. 3(a)) was obtained by inserting an oversized steel pin into the hole of an open hole specimen. The material of the pin was made of AISI-D2 steel. The interference fit level is defined as $I = (d_2 - d_1)/d_1 \times 100\%$, where d_1 is the diameter of the hole and d_2 is the large diameter of the pin. Fig. 3(b) shows the dimensions of the pin causing an interference fit of 2%. Fatigue tests were performed at seven different maximum

Table 1
Maximum cyclic loading for the specimens with cold expanded hole.

P_{max} (kN)	14.63	16.88	19.13	21.38	23.65	25	27	29.03
Maximum remote stress (MPa)	130	150	170	190	210	222	240	258

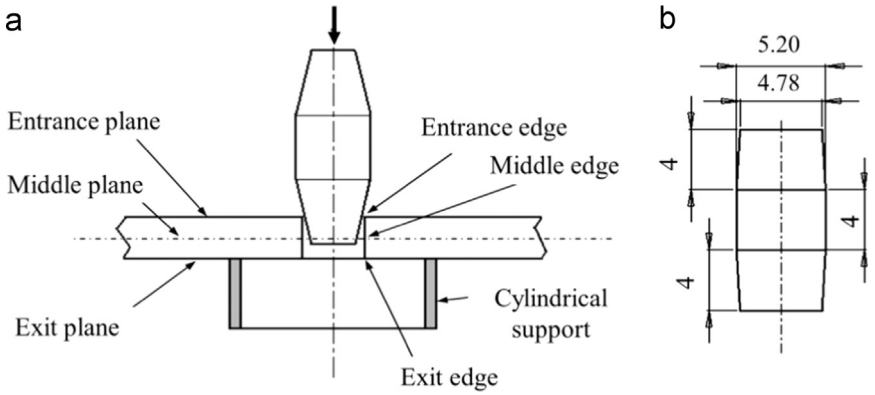

Fig. 2. (a) Schematic of the hole cold expansion process, (b) dimensions of the pin (mm) [28].

Fig. 3. The pin interference fitted specimens (a) and (b) the dimensions of pin for 2% interference fit [29].

Table 2
Maximum cyclic loading for the pin interference fitted specimens.

P_{max} (kN)	29	31	33	35	37	39	41
Maximum remote stress (MPa)	258	275.5	293.3	311.1	328.8	346.6	364.4

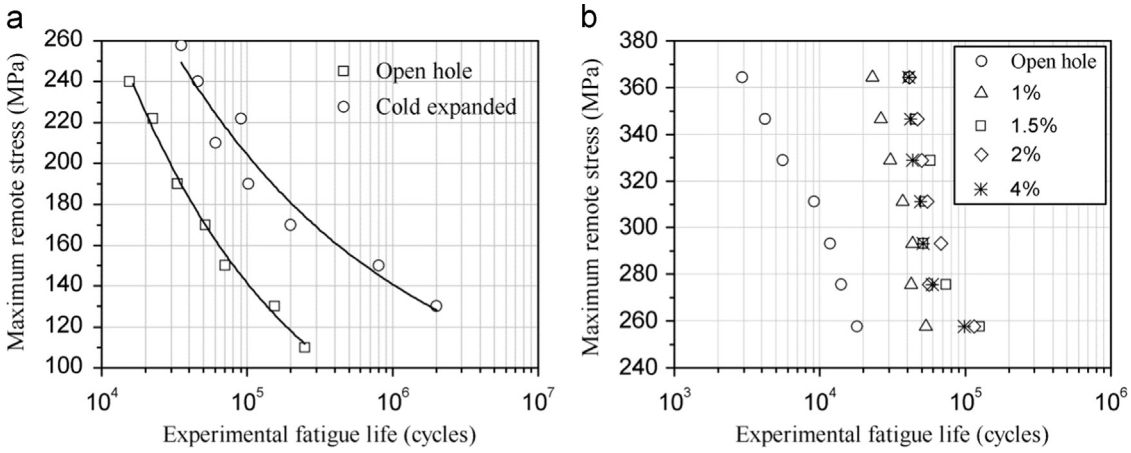

Fig. 4. Experimental stress-life data for: (a) open hole and cold expanded specimens [28], (b) open hole and pin interference fitted specimens [2].

loads, as shown in Table 2, and the experimental results are shown in Fig. 4(b).

3. Theoretic models

In order to investigate the effect of cold expansion and pin interference fit on fatigue life of a fastener hole, two phases of analysis need to be carried out. The first one is the calculation of the residual stresses and initial plasticity damage after hole cold expansion or interference fit, in which the damage-coupled Chaboche plasticity constitutive model and plasticity damage model are the basis of the analysis. The second one is the analysis of fatigue damage evolution of the plate under cyclic loading, in which the elasticity and plasticity damage models and damage cumulative rule are utilized for the simulation.

3.1. Damage-coupled Chaboche plasticity constitutive model

To model the behavior of a damaged and hardened plastic material, the damage-coupled plasticity constitutive model proposed by Lemaitre and Chaboche [23] is used.

A Representative Volume Element (RVE) [23] is introduced to describe the deterioration of the material under external loading. The properties of the RVE are represented by homogenized variables. The typical dimension of a RVE is near 0.1 mm for metals. In this study, it is assumed that damage is isotropic and can be represented by a decrease in the elastic modulus [23]. The damage variable is thus defined as follows:

$$D = 1 - E/E_0 \tag{1}$$

where E is the equivalent elastic modulus of the damaged RVE, and E_0 is the initial elastic modulus of the material. Considering a small deformation, the total strain ε_{ij} can be decomposed as:

$$\varepsilon_{ij} = \varepsilon_{ij}^e + \varepsilon_{ij}^p \tag{2}$$

where ε_{ij}^e and ε_{ij}^p are the elastic and plastic strains, respectively. According to the principle of strain equivalence [23], the elastic strain takes the form:

$$\varepsilon_{ij}^e = \frac{1+\nu}{E_0}\frac{\sigma_{ij}}{1-D} - \frac{\nu}{E_0}\frac{\sigma_{kk}}{1-D}\delta_{ij} \tag{3}$$

where ν is Poisson's ratio, σ_{ij} is the Cauchy stress, and δ_{ij} is the Kronecker delta.

The von Mises yield function including damage is expressed by:

$$f = \sqrt{\frac{3}{2}\left(\frac{s_{ij}}{1-D} - \alpha_{ij}\right)\left(\frac{s_{ij}}{1-D} - \alpha_{ij}\right)} - Q \tag{4}$$

where s_{ij} is the deviatoric part of the stress, α_{ij} is the deviatoric part of the back stress, and Q is the radius of the yield surface and

its evolution is defined as:

$$\dot{Q} = \dot{\lambda} b(Q_\infty - Q) \tag{5}$$

where b and Q_∞ are material constants, $\dot{\lambda}$ is the plastic multiplier that is determined by the plastic flow consistency condition: $\dot{f} = f = 0$. The nonlinear kinematic hardening model (NLKH) proposed by Chaboche [30] is used to represent the kinematic hardening behavior.

$$\alpha_{ij} = \sum_{k=1}^{M} \alpha_{ij}^{(k)} \tag{6}$$

The evolution of the plastic strain components [23] can be obtained as

$$\dot{\varepsilon}_{ij}^{p} = \frac{3}{2}\frac{\dot{\lambda}}{1-D}\left(\frac{s_{ij}}{1-D} - \alpha_{ij}\right) \Big/ \left(\frac{s_{ij}}{1-D} - \alpha_{ij}\right)_{eqv} \tag{7}$$

$$\dot{p} = \sqrt{\frac{2}{3}\dot{\varepsilon}_{ij}^{p}\,\dot{\varepsilon}_{ij}^{p}} = \frac{\dot{\lambda}}{1-D} \tag{8}$$

$$\dot{\alpha}_{ij}^{(k)} = \left(\frac{2}{3}C_k\dot{\varepsilon}_{ij}^{p} - \gamma_k\alpha_{ij}^{(k)}\dot{p}\right)(1-D) \tag{9}$$

where $\dot{p}$ is the accumulated plastic strain rate. In Eq. (9), C_k and γ_k are material constants that are determined from experimental tests.

3.2. Damage evolution models

Based on the stress-controlled low-cycle fatigue tests performed by Kang [24], the damage D can be considered to occur in two parts: elasticity and plasticity damage, which are dependent on the cyclic stress and accumulated plastic strain, respectively. Thus:

$$D = D_e + D_p \tag{10}$$

3.2.1. Plasticity damage model

The evolution law [31] of the plasticity damage D_p considering the stress triaxiality effect is given by:

$$\dot{D}_p = \left(\frac{\sigma_{eqv}^2 R_v}{2E_0 S(1-D_p)^2}\right)^m \dot{p} \tag{11}$$

$$R_v = \tfrac{2}{3}(1+\nu) + 3(1-2\nu)(\sigma_H/\sigma_{eqv})^2 \quad \text{if} \quad \sigma_H \geq 0 \tag{12}$$

where S and m are material parameters, R_v is the stress triaxiality function, and σ_H and σ_{eqv} are the hydrostatic and von Mises stresses, respectively. Due to the limited knowledge present in the literature, the damage mechanism in the state of compressive stress is not currently clear. To extend the plasticity damage model into the state of compressive stress, a conservative method is used in this study. The stress triaxiality function in the state of compressive stress is:

$$R_v = \tfrac{2}{3}(1+\nu) \quad \text{if} \quad \sigma_H < 0 \tag{13}$$

3.2.2. Elasticity damage model

The thermodynamic formulation for the elasticity damage has been described in [23]. For the case of multiaxial cyclic loading, the damage rate equation of the non-linear continuous damage model (NLCD) can be written as:

$$\dot{D}_e = \frac{dD}{dN} = \left[1-(1-D)^{\beta+1}\right]^{\alpha} \cdot \left[\frac{A_{II}}{M_0(1-3b_2\sigma_{H,mean})(1-D)}\right]^{\beta} \tag{14}$$

where N is the number of cycles until failure; β, M_0 and b_2 are material constants that are determined by fatigue tests; A_{II} is the amplitude of an octahedral shear stress, which is expressed by:

$$A_{II} = \frac{1}{2}\left[\frac{3}{2}(S_{ij,\,max} - S_{ij,\,min}) \cdot (S_{ij,\,max} - S_{ij,\,min})\right]^{1/2} \tag{15}$$

where $S_{ij,\,max}$ and $S_{ij,\,min}$ are the maximum and minimum values of the deviatoric stress tensor ij components during one loading cycle. In Eq. (14), $\sigma_{H,mean}$ is the mean hydrostatic stress, which is defined by:

$$\sigma_{H,mean} = \frac{1}{2}(\sigma_{H,\,max} + \sigma_{H,\,min}) \tag{16}$$

where $\sigma_{H,\,max}$ and $\sigma_{H,\,min}$ are the maximum and minimum hydrostatic stresses during one loading cycle. Also in Eq. (14), the parameter α is given by:

$$\alpha = 1 - a\left\langle \frac{A_{II} - A_{II}^*}{\sigma_u - \sigma_{eqv,\,max}} \right\rangle \tag{17}$$

where $\sigma_{eqv,\,\max}$ is the maximum von Mises stress during one loading cycle. The Sines fatigue limit criterion [32] in this model is formulated as:

$$A_{II}^* = \sigma_{l0}(1 - 3b_1\sigma_{H,mean}) \tag{18}$$

where σ_{l0} is the fatigue limit at zero mean stress and b_1 is a material constant.

The number of cycles until failure is given by integrating Eq. (14) between $D = 0$ and $D = 1$:

$$N_F = \frac{1}{1+\beta} \cdot \frac{1}{aM_0^{-\beta}} \cdot \frac{\langle \sigma_u - \sigma_{eqv,\,max} \rangle}{\langle A_{II} - A_{II}^* \rangle} \cdot \left[\frac{A_{II}}{1 - 3b_2\sigma_{H,mean}}\right]^{-\beta} \tag{19}$$

3.3. Critical plane SWT model

The Smith–Watson–Topper [17] critical plane criterion is used, for comparative purposes, to estimate the fatigue life. This criterion is based on the experimental observations that the critical fatigue crack occurs at a specified plane and the fatigue life is controlled by the maximum tensile stress and strain amplitude on the specified plane. The SWT life prediction employs a combined low-cycle and high-cycle fatigue equation, which is expressed by:

$$\sigma_{n,\,max}\frac{\Delta\epsilon_1}{2} = \frac{(\sigma_f')^2}{E_0}(2N_f)^{2b} + \sigma_f'\epsilon_f'(2N_f)^{b+c} \tag{20}$$

where $\sigma_{n,\,\max}$ and $\Delta\epsilon_1$ are the maximum normal stress and principle strain range on the critical plane, σ_f' and b are the high-cycle fatigue constants, ε_f' and c are the low-cycle fatigue constants.

3.4. Identification of material parameters

In this study, three groups of parameters need to be identified according to the experimental data. Experimental data from uniaxial tensile tests, low-cycle and high-cycle fatigue tests are required in the identification of material parameters. The least squares method is used to determine the material parameters based on the data in the MIL-HDBK-5H handbook [33,34]. The methodology and result are briefly introduced as below.

3.4.1. Identification of material parameters in the plasticity constitutive equations

Firstly, from the uniaxial tensile test, the parameters in the constitutive equations can be obtained. Isotropic hardening is neglected in this study. Three components of the back stress ($M = 3$) are used. The components of the back stress can be expressed as an exponential saturation equation, thus the

stress–strain curve is expressed as:

$$\sigma = \sigma_y + \sum_{k=1}^{M} \frac{C_k}{\gamma_k}(1 - e^{-\gamma_k \varepsilon_p}) \tag{21}$$

where σ_y and ε_p are the initial yield stress and the plastic strain, respectively. Fig. 5 shows the fitting curve of the stress–strain curve, and the parameters are summarized in Table 3.

3.4.2. Identification of material parameters in the plasticity damage model

Secondly, the parameters m and S are determined from the strain-controlled low-cycle fatigue test data. Using the Coffin–Manson relationship, the strain-life curve can be written as:

$$\frac{\Delta\epsilon_p}{2} = \epsilon_f'(2N_F)^c \tag{22}$$

where ε_f' and c are material parameters. Using the cyclic stress–strain curve described by:

$$\sigma_{\max} = H'(\Delta\epsilon_p/2)^{n'} \tag{23}$$

where H' and n' are parameters determined from experiments. For the uniaxial case, the number of cycles until failure is found by integrating Eq. (11) between $D=0$ and D_c:

$$N_F = \frac{1-(1-D_c)^{2m+1}}{2(2m+1)}\left(\frac{2^{1+2n'}ES}{H'^2}\right)^m (\Delta\epsilon_p)^{-(1+2mn')} \tag{24}$$

where D_c is the critical value of the damage at macrocrack formation. The parameter D_c is determined from a tension test, the details has been described in the literature [27]. The values of ε_f', c, H' and n' are obtained from strain-based fatigue tests data [34]. The material parameters in Eqs. (11) and (24) are obtained by equating Eqs. (22) and (24), and are shown in Table 4.

3.4.3. Identification of material parameters in the NLCD and SWT model

Lastly, the stress-life curve [34] of unnotched specimens for Al alloy 7075-T6 are used to identify the parameters of the NLCD model. The fatigue limit σ_{l0} and b_1 are obtained from stress-life data at different stress ratios (e.g., $R=-1$, 0 and 0.5). The values of M_0 and β can be determined numerically by stress-life data at stress ratio$R=-1$, b_2 can be determined from stress-life data at different stress ratios (e.g., R=0 and 0.5). Based on the known values of $aM_0^{-\beta}$and β, a can be identified numerically. The details of this method have been described by Zhang [25]. The identified material parameters are shown in Table 5.

Besides, the stress-life curve [34] is also used in the SWT model. The material parameters of SWT are shown in Table 6. Fig. 6 shows the comparison of the SWT model and the integrated NLCD model for uniaxial fatigue at different stress ratios.

4. Finite element models and numerical simulation scheme

4.1. Finite element models

One eighth of the open hole specimen was modeled using symmetric boundary conditions at the three planes of symmetry,

Table 4
Material parameters of the plasticity damage model for Al alloy 7075-T6.

S	m	D_c	ε_f'	c	H'	n'
7.90	2.88	0.10	0.262	-0.619	977	0.106

Table 5
Material parameters of the NLCD model for Al alloy 7075-T6.

β	$aM_0^{-\beta}$	b_1	b_2	σ_{l0}	a
3.80	2.243×10^{-15}	0.0015	0.0012	46 MPa	0.70

Table 6
Material parameters of the SWT model for Al alloy 7075-T6.

σ_f' (MPa)	ε_f'	b	c
1466	0.262	−0.143	−0.619

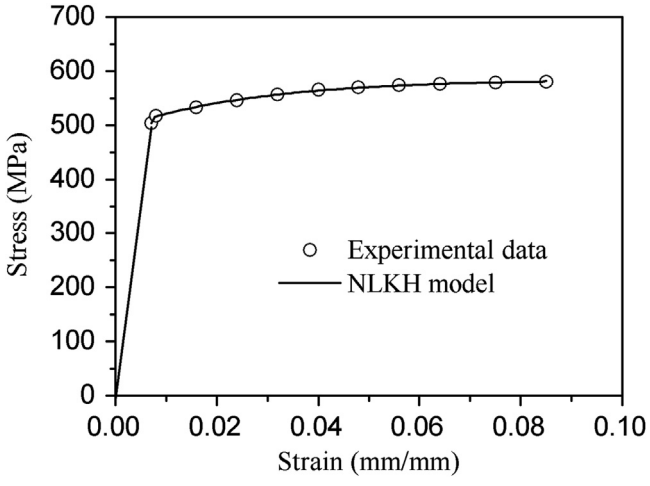

Fig. 5. Stress–strain curve for Al alloy 7075-T6.

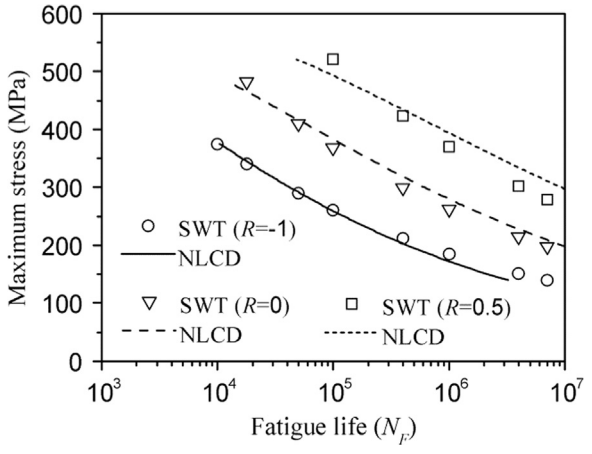

Fig. 6. Fatigue life comparison between the integrated NLCD and SWT model.

Table 3
Static mechanical and material parameters for Al alloy 7075-T6.

E(MPa)	ν	σ_y(MPa)	σ_u(MPa)	C_1(MPa)	C_2(MPa)	C_3(MPa)	γ_1	γ_2	γ_3
71,500	0.33	503	600	784.3	1743.2	126,767.4	34.5	34.7	11,840

as shown in Fig. 7. In the hole cold expansion and pin interference fit processes, a quarter of the specimens are modeled, and symmetric boundary conditions are used in X–Z and Y–Z Cartesian planes. The models of hole cold expansion and interference fitted specimens consist of two sets of elements for the plate and pin. The 3D 8-node solid elements (C3D8 in ABAQUS) are used to mesh the models. The contacts between the pin and plate are defined using the master-slave algorithm for contact between surfaces. These contacts allow the pressure to be transferred between the contacting surfaces, and without them the contacting areas penetrate each other. The sizes of the elements are refined with the smallest width of 0.05 mm around the hole. The damage-coupled Chaboche constitutive model is used to simulate the stress–strain behavior of Al-alloy 7075-T6. For the pins, a linear elastic material behavior is used with an elastic modulus of 207 GPa and a Poisson's ratio of 0.3. Coulomb friction is used to simulate the friction behavior between the contact surfaces with a coefficient of $\mu=0.1$.

Two primary steps are included in the numerical simulations: model the hole cold expansion or pin interference fit processes; model the fatigue damage processes. In the simulation of the cold expansion process, the pin is pulled passing through the hole by applying an incremental displacement on the upper surface of the pin in the Z direction. In the simulations of interference fit process, the pin is inserted into the hole and kept in the hole. In the simulations of fatigue damage, cyclic loading is applied on the models. Due to the pin being removed after hole cold expansion, the cold expanded specimens in fatigue damage simulation is performed in the same manner as for the open hole plate. For the interference fitted models, the pin is kept in the hole during the fatigue damage simulation.

4.2. Numerical simulation scheme

User material subroutines are used to implement the damage-coupled Chaboche constitutive model and the damage evolution equations. In the fatigue damage simulations, the subroutine updates the stress and solution-dependent variables and the Jacobian matrix at each time increment, and calculates the damage rata and accumulation at each integration point during the cycles. Because significant amounts of computation time are required to simulate each fatigue cycle, a cycle jumping factor ΔN is introduced to reduce the number of cycles actually being calculated. It is assumed that the cyclic stresses and the accumulated plastic strain and damage remain unchanged during each block of ΔN cycles. Take for example the simulation for the specimen with cold expanded hole, the simplified algorithm is shown in Fig. 8. The details of the numerical simulation scheme are listed as follows:

1. The hole cold expansion process is simulated, and the corresponding plastic damage is calculated as the initial damage $D^{(0)}$ according to Eq. (11).

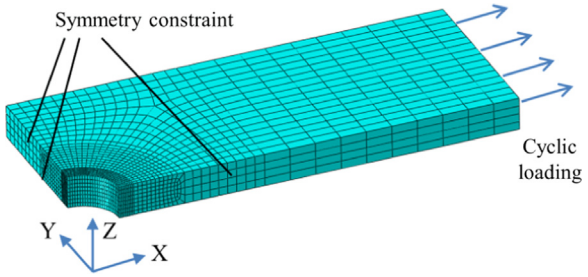

Fig. 7. Finite element model for open hole specimen.

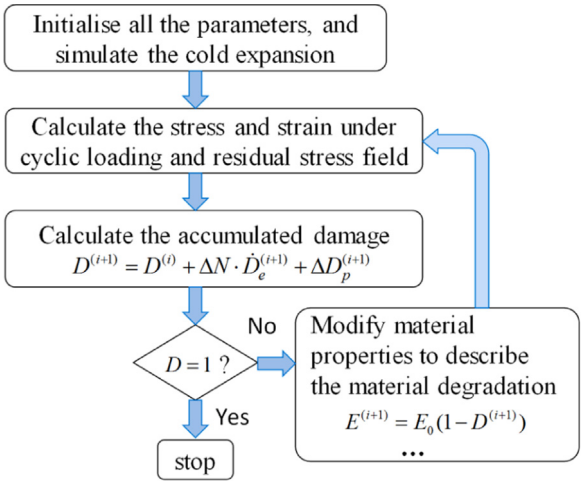

Fig. 8. Simplified algorithm of the numerical simulation.

2. The cyclic stress and the accumulated plastic strain are calculated under cyclic loading.
3. The fatigue damage is calculated based on Eqs. (11) and (14) after ΔN cycles, the accumulated damage given as:

$$D^{(i+1)} = D^{(i)} + \Delta N \cdot \dot{D}_e^{(i+1)} + \Delta D_p^{(i+1)} \tag{25}$$

The plastic damage $\Delta D_p^{(i+1)}$ is dependent on whether cyclic plasticity occurs during the cycles. If cyclic plasticity occurred, the plastic damage is calculated ΔN times; otherwise, the plastic damage is assumed to have occurred at the first cycle of the ΔN cycles.

$$\Delta D_p^{(i+1)} = \begin{cases} \Delta N \cdot \dot{D}_p^{(i+1)} & \textit{cyclic plasticity} \\ \dot{D}_p^{(i+1)} & \textit{else} \end{cases} \tag{26}$$

4. The material properties of the damaged element are modified to account for the material degradation:

$$E^{(i+1)} = E^{(i)}(1 - D^{(i+1)}) \tag{27}$$

$$C_k{}^{(i+1)} = C_k{}^{(i)}(1 - D^{(i+1)}) \tag{28}$$

$$\gamma_k{}^{(i+1)} = \gamma_k{}^{(i)}(1 - D^{(i+1)}) \tag{29}$$

5. The algorithm repeats steps (2)–(4) until the damage of any integration points reaches a value of 1, which indicates that a fatigue crack has formed.

5. Results and discussions

5.1. Residual stress and initial plasticity damage

Fig. 9 shows the circumferential residual stress field around the hole after the cold expansion. The highest compressive residual stress is shown to be localized near the mid-thickness of the specimen with a maximum magnitude of 598 MPa, the exit and entrance faces experience lower compressive residual stresses. Fig. 10 shows the residual stress distribution on the entrance and exit face, and the middle-thickness along the direction of depicted in Fig. 9. Compressive residual stress is shown near the hole edge, and tensile residual stress is shown beyond the region of compressive residual stress.

Fig. 11 shows the distribution of the accumulated plastic strain and the associated plastic damage after hole cold expansion. The distributions of the plastic strain and damage are both symmetrically distributed along the circumference of the hole. The maximum plastic strain exits near the exit edge with a magnitude of 0.129. The maximum damage appears near the exit edge with a magnitude of 0.0016. The distributions of the plastic strain and damage are related to the stress triaxiality that occurs during the hole cold expansion process.

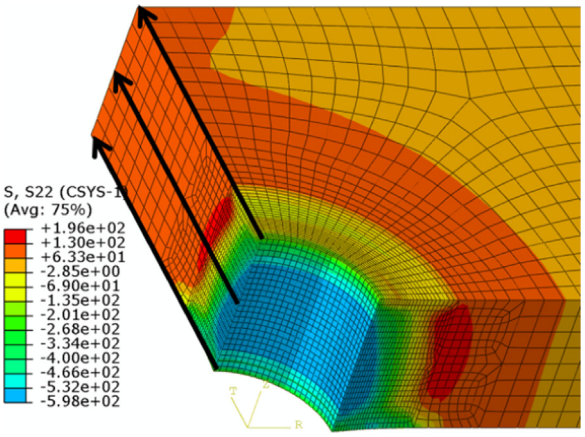

Fig. 9. Contour of circumferential residual stress (MPa) after hole cold expansion.

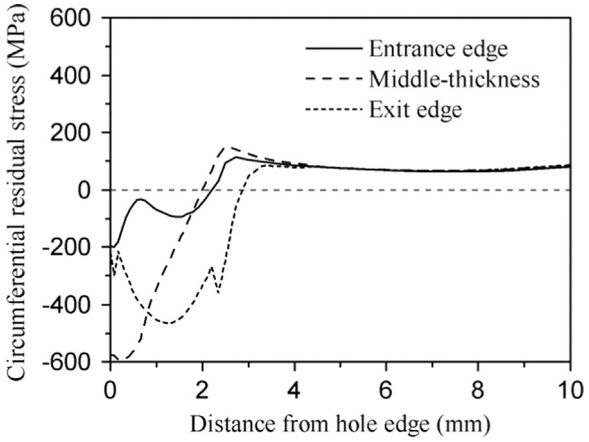

Fig. 10. Distribution of circumferential residual stress after hole cold expansion.

Fig. 12 shows the circumferential residual stress field around the hole after the pin was inserted in the hole with interference fit of 2%. Compressive and tensile residual stress both exist near the hole surface, with the highest tensile residual stress being localized at the exit edge. Fig. 13 shows the residual stress on the entrance and exit face, and the middle-thickness. Tensile residual stress is shown to play a major role around the hole, except at the region near the middle-thickness.

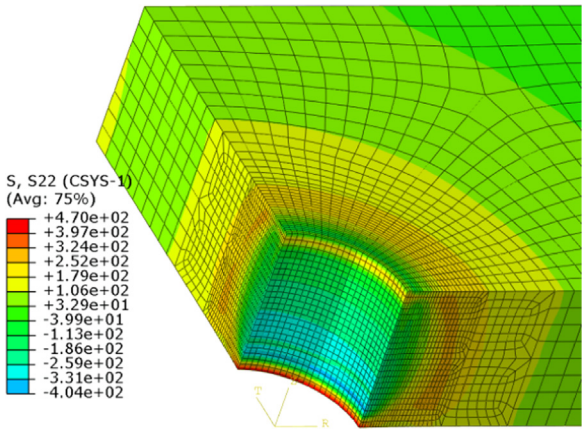

Fig. 12. Contours of circumferential residual stress (MPa) after pin interference fit of 2%.

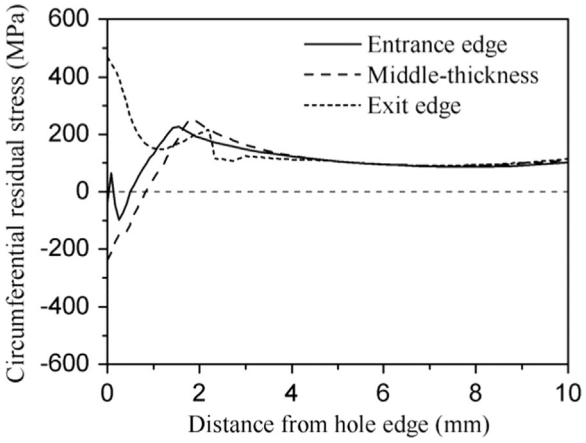

Fig. 13. Distribution of circumferential residual stress after pin interference fit of 2%.

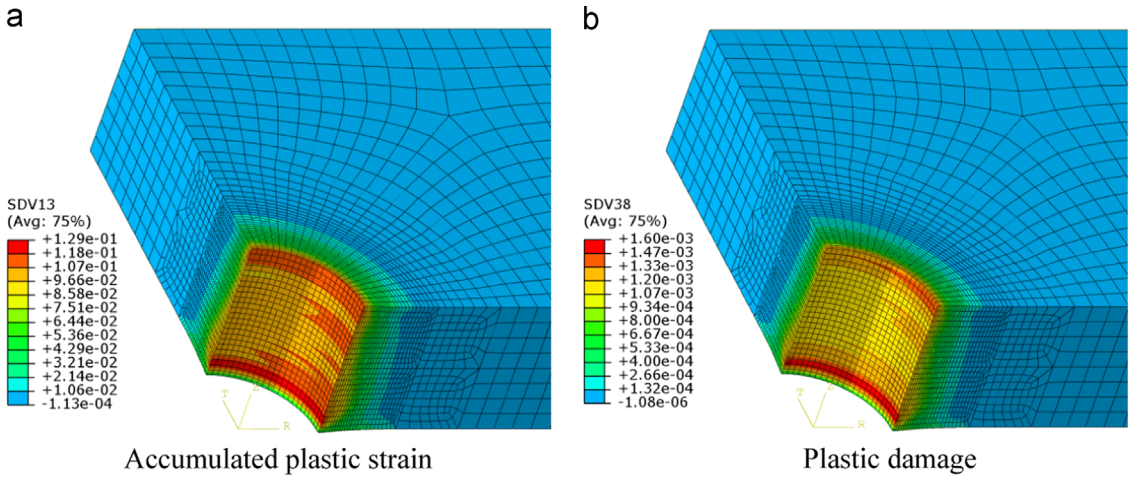

Fig. 11. Distribution of: (a) accumulated plastic strain, and (b) plastic damage after hole cold expansion.

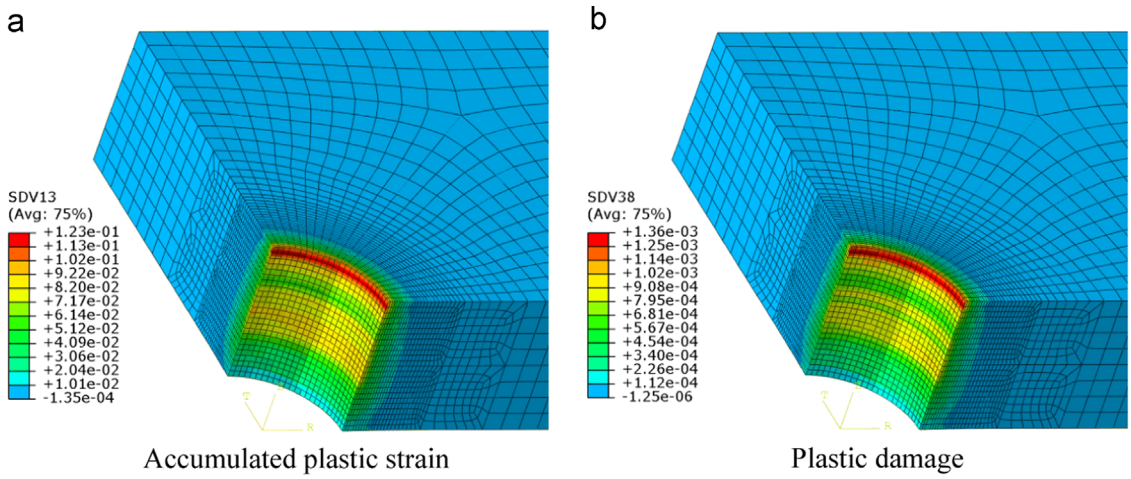

Fig. 14. Distribution of: (a) accumulated plastic strain and (b) plastic damage after pin interference fit of 2%.

Table 7
Predicted fatigue lives using different ΔN for an open hole specimen. under maximum stress of 240 MPa.

ΔN	50	100	250	500	1000
N_F	10,750	10,800	11,000	11,500	12,000
$\Delta N/N_F$	0.0056	0.014	0.028	0.056	0.085

Fig. 14 shows the distribution of the accumulated plastic strain and the plastic damage after pin interference fit. The plastic strain and damage are symmetrically distributed along the circumference of the hole. The maximum plastic strain is shown to be localized near the entrance edge with a magnitude of 0.123. The maximum damage is also shown to be localized near the entrance edge with a magnitude of 0.00136. The distributions of the plastic strain and damage are related to the stress triaxiality that occurs during the pin interference fit process.

5.2. Predicted fatigue damage results

5.2.1. Predicted fatigue lives and crack nucleation locations

Three different methods were used to predict the fatigue life of the specimens after the analysis of hole cold expansion or pin interference fit process, as follows:

1. The critical plane SWT method calculates the fatigue life using the SWT model (Eq. (20)) and cyclic stresses obtained from FE analysis of a stabilized fatigue cycle.
2. The integrated NLCD method calculates the fatigue life using the integrated NLCD model (Eq. (19)) and cyclic stresses obtained from FE analysis of a stabilized fatigue cycle, without coupled damage accumulation.
3. The proposed approach predicts the fatigue life using the FE model coupled with incremental damage accumulation and associated material degradation, in which the damage is calculated based on Eq. (11) and the NLCD model (Eq. (14)).

The cycle jumping factor ΔN can thus affect the predicted fatigue life. The convergence of the numerical simulation scheme was verified using an open hole specimen at a maximum stress level of 240 MPa. Five values of ΔN (e.g., 50, 100, 200, 400 and 1000) were used to calculate the fatigue lives of the specimen. Table 7 shows the predicted lives N_F at different values of ΔN. It is shown that a convergent result can be obtained when $\Delta N/N_F < 0.02$.

Fig. 15 shows the predicted fatigue lives versus the experimental results (Fig. 4(a)) for the open hole and hole cold expanded specimens. As shown in Fig. 15(a), the proposed approach predict the fatigue lives accurately, while the integrated NLCD and SWT model both underestimates the fatigue lives especially at high stress levels. For the hole cold expanded specimens (Fig. 15(b)), the proposed approach and SWT model are shown to give better overall agreement with the experimental data, while the integrated NLCD underestimates the fatigue lives. Fig. 16 shows the predicted life versus the experimental life (Fig. 4(b)) for the pin interference fit specimens with interference fit level of 2% and 4%. As shown, the predicted fatigue lives using the proposed approach are in good agreement with experimental results, while the integrated NLCD provides underestimated predictions. The SWT model results are generally in agreement with experimental results, but the results show significant deviation at high stress levels.

The error index (ER) is used to evaluate the deviation between the predicted lives and experimental fatigue lives [35]:

$$\mathrm{ER} = \log\left(N_{\mathrm{predicted}}/N_{\mathrm{experimental}}\right)$$

$$\overline{\mathrm{ER}}\% = \left(\frac{1}{n}\sum_{i=1}^{n}|\mathrm{ER}_i|\right)\times 100 \tag{30}$$

Table 8 presents the average absolute errors of different life prediction methods. It is shown that the error of the proposed approach is the smallest, while the error of the integrated NLCD is the largest. The proposed approach shows significantly superior performance to the integrated NLCD and SWT results. The CDM coupled with FE analysis provides an insight into fatigue damage evolution and stress redistribution at the critical location and hence predicts longer lives compared with the integrated formula (Table 8).

Fig. 17 shows the predicted damage fields and crack nucleation locations for the open hole, hole cold expanded and pin interference fit specimens. For the open hole specimens under a remote stress of 240 MPa (Fig. 17(a)), the predicted crack is shown to nucleate at the median-thickness of the hole surface. For the hole cold expanded specimens under a remote stress of 258 MPa (Fig. 17(b)), the crack is predicted to nucleate from the entrance edge at the smallest section within a small region. The predicted result for the hole cold expanded specimens shows good agreement with the experimental result in Fig. 18(a). For the pin interference fit specimen experiencing a remote stress of 311.1 MPa, the crack is predicted to nucleate from the entrance edge within a relatively large region, which agrees well with the experimental

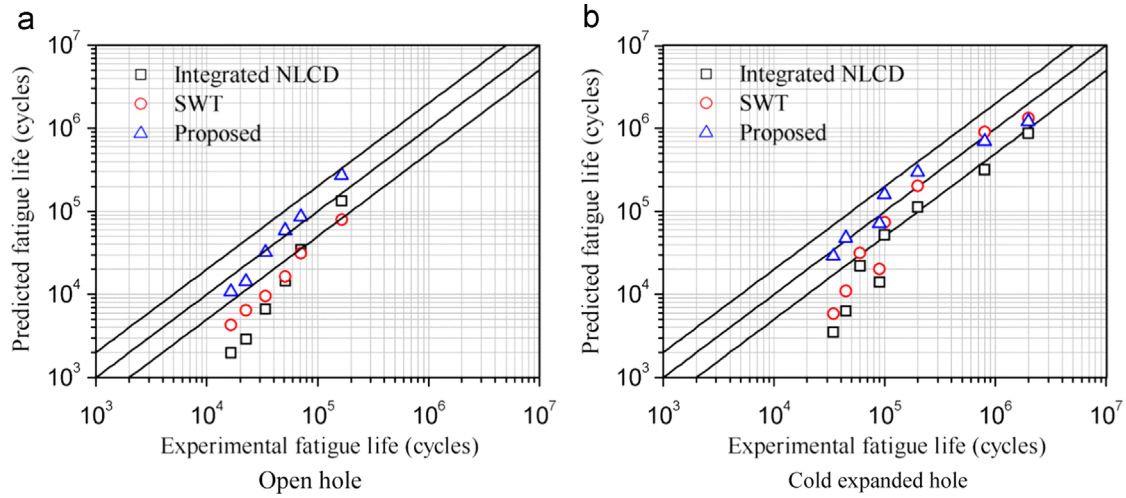

Fig. 15. Comparison of the experimental and predicted fatigue lives for (a) open hole and (b) hole cold expanded specimens.

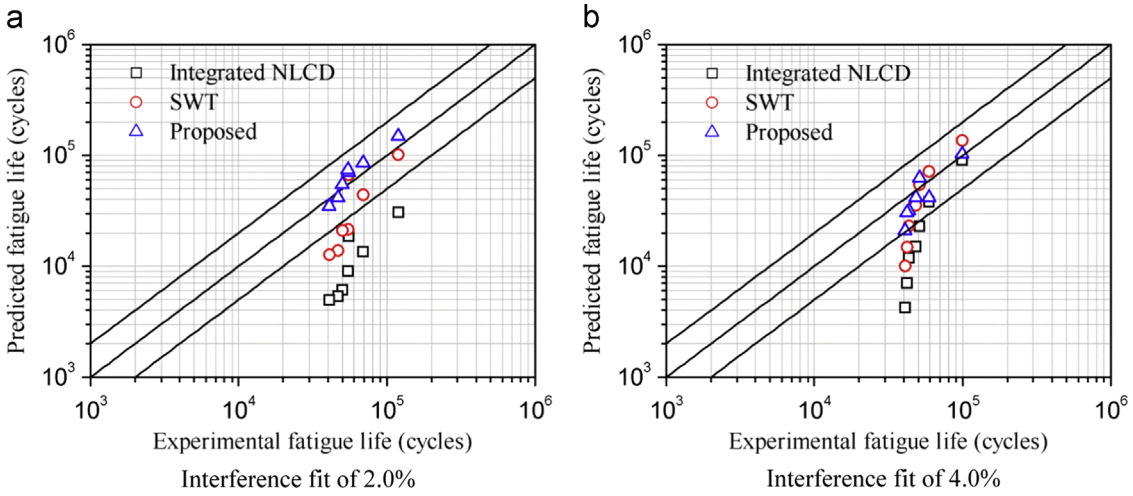

Fig. 16. Comparison of the experimental and predicted fatigue lives for specimens with pin interference fit of: (a) 2.0% and (b) 4.0%.

Table 8
The average absolute errors of different life prediction methods.

	Open hole	Hole cold expansion	Interference fit 2%	Interference fit 4%
SWT	47.6	33.4	24.6	31.1
Integrated NLCD	58.1	54.6	48.9	76.2
Proposed	14.2	12.3	12.5	8.2

result in Fig. 18(b). Moreover, damage is shown to occur in the smallest cross section, which is explained by the fact that material in this region is prone to damage due to the combined effect of tensile residual stress and cyclic stress.

5.2.2. Predicted stress–strain curve and damage accumulation

Fig. 19 shows the longitudinal stress–strain curves at the crack nucleation location for the open hole, hole cold expanded and pin interference fit specimens under a remote stress of 258 MPa. For the open hole specimens (Fig. 19(a)), the maximum stress σ_X is shown to decrease as the number of loading cycles increases, which can be attributed to the stress redistribution due to the accumulated fatigue damage. It is also shown that cyclic plastic strain occurs at the end of the simulation due to fatigue damage and softening of the material. The strain ε_X is shown to increase significantly, which is a result of the reduction in the stiffness. For the hole cold expanded specimen (Fig. 19(b)), the maximum stress σ_X is shown to decrease with an increasing number of loading cycles. The stress–strain hysteresis loop remains approximately linear during the fatigue cycling, which indicates that an elastic damage evolution for the specimens is predominant. For the pin interference fit specimen (Fig. 19(c)), plastic strain occurs during the first cycle, the maximum values of σ_X is also shown to decrease as the number of cycles increases. The stress–strain hysteresis loop is also shown to be linear during the fatigue cycling. Opposite to the open hole specimen, the maximum strain and strain amplitude of the hole cold expanded and pin interference fit specimens are shown to change little during the fatigue cycling. It is explained that the damage of the hole cold expanded and pin interference fit specimens are localized within a small region, and that the adjacent material produced much smaller damage due to significant residual stress, thus the maximum strain ε_X is shown to change little during the fatigue cycling. Fig. 20 shows the predicted damage accumulation for the open hole, hole cold expanded and pin interference fit specimens under a remote stress of 258 MPa. For the open hole specimen, the damage is shown to be low initially, but accumulates rapidly as the number of loading cycles increases. For the cold expanded specimen, the damage is shown to accumulate rapidly at the beginning of the fatigue cycling, but accumulates smoothly as the number of cycles increases. For the

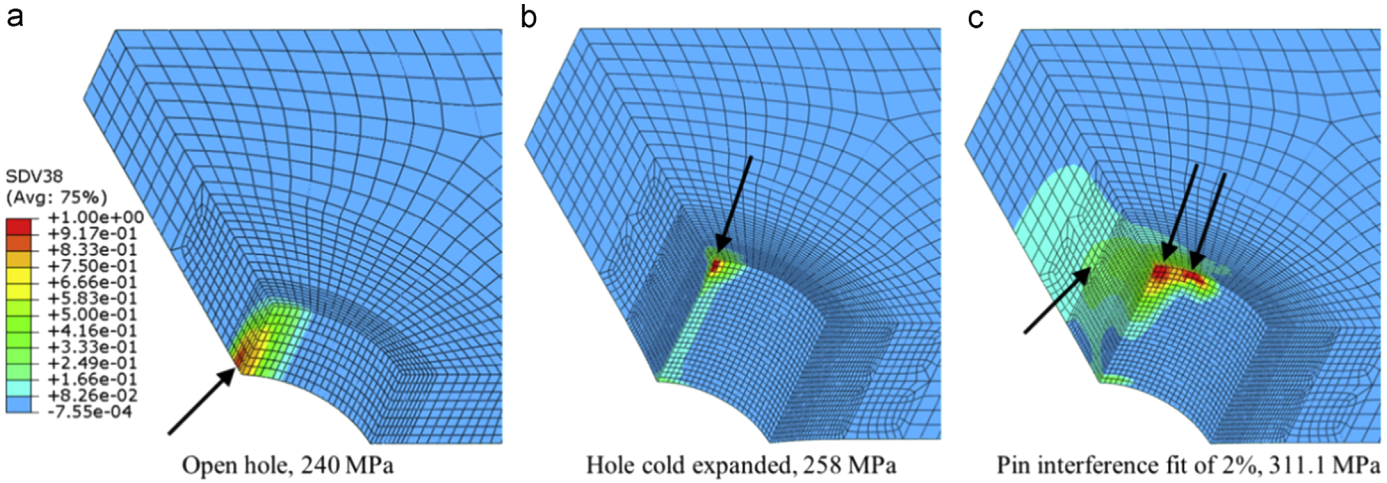

Fig. 17. Predicted damage field and fatigue crack nucleation locations for different specimens.

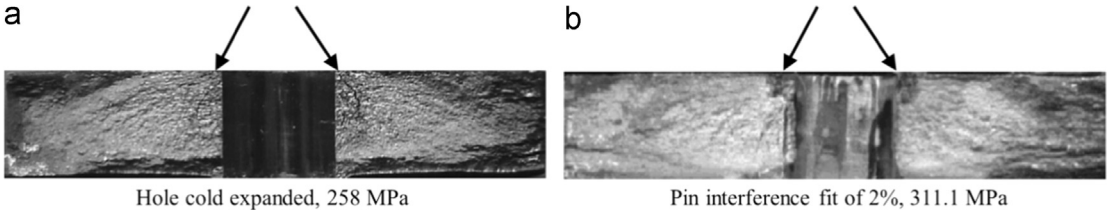

Fig. 18. Experimental fatigue crack nucleation location for the hole cold expanded [28] and pin interference fit [2] specimens.

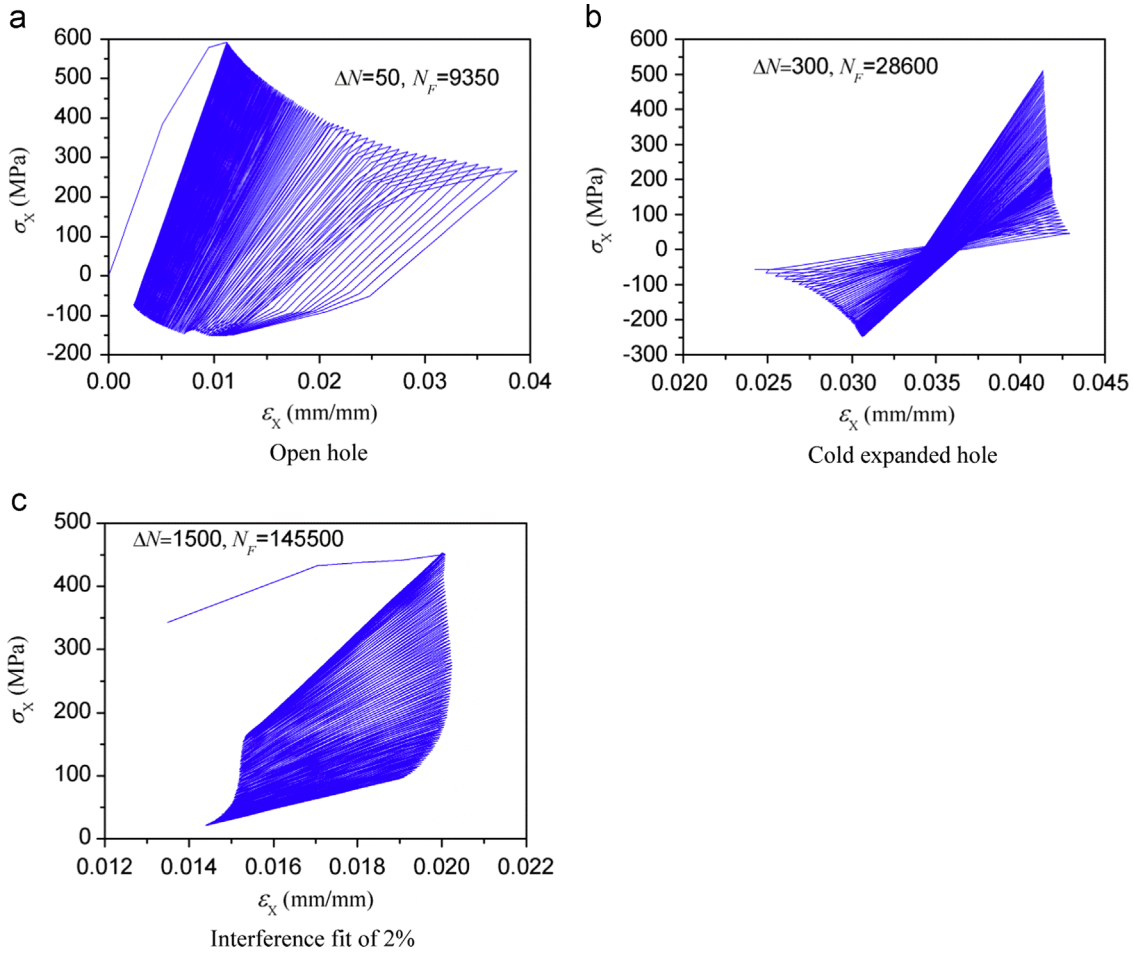

Fig. 19. Stress–strain curve of integration points at crack nucleation location for: (a) open hole, (b) hole cold expanded and (c) pin interference fit specimens.

pin interference fit specimen, the damage is shown to accumulate smoothly as the number of loading cycles increases. The damage accumulation curves of the hole cold expanded and pin interference fit specimens remain approximately as a line during the fatigue cycling, while the curve of the open hole presents sharply rising toward the end of the fatigue cycling. According to the principle of strain equivalence [27], the strain constitutive equation of a damaged material is derived from the same formalism as for a non-damaged material. Therefore, the increasing strain and strain amplitude in the damage evolution of open hole specimen will yield increasing damage accumulation rate; while the constant strain and strain amplitude in the damage evolution of hole cold expanded or pin interference fit specimen will yield constant damage accumulation rate. It can be concluded that the cyclic stress–strain at the crack nucleation location of the hole cold expanded and pin interference fit specimens will be beneficial to the fatigue life improvement. Moreover, the initial plasticity damage that occurs during the hole cold expansion or pin interference fit process is relatively small in comparison to the critical value of fatigue crack nucleation of $D=1$, which has little influence on fatigue life of the specimens.

The beneficial effect of hole cold expansion and interference fit is not only due to the reduction in maximum stress or stress amplitude, but also because of the change in the damage evolution at the critical location. Based on the simulation results, the effects of hole cold expansion and interference fit on the fatigue life improvement of fastener hole are summarized as follows:

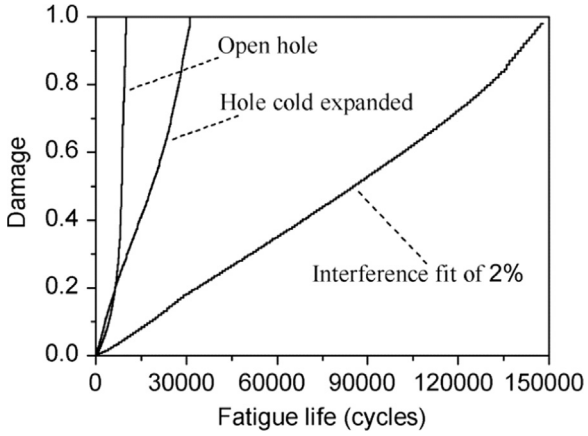

Fig. 20. Predicted damage accumulation for the open hole, hole cold expanded and pin interference fit specimens.

1. The hole cold expansion and pin interference fit reduce the maximum stress and the stress amplitude at the critical position, respectively.
2. The initial plasticity damage that occurs during the hole cold expansion and pin interference fit process has little influence on fatigue life in this study.
3. The damage evolutions of hole cold expanded and pin interference fit specimens are dominated by elastic damage during the fatigue process.

5.2.3. Effect of the hole cold expansion and pin interference fit on cyclic stress

To investigate the level of hole cold expansion and cyclic loading on fatigue life improvement, the longitudinal stress σ_X at the entrance edge for the open hole and five batches of cold expanded hole (ranging from 2% to 6%) specimens under maximum stress of 150 and 258 MPa are shown for two cycles in Fig. 21, in which the maximum loads are exerted at the time of the end of the first half and the third half of the fatigue cycling. For the 150 MPa case (Fig. 21(a)), the maximum stresses σ_X of five batches of cold expanded hole specimens are shown to be reduced by more than 300 MPa. As the cold expansion level is increased, the maximum stress is shown to have little additional decrease. For the 258 MPa case (Fig. 21(b)), the maximum stresses of five batches of cold expanded hole specimens are shown to be reduced by less than 150 MPa. The maximum stress shows little additional decrease as the cold expansion level increases. The reduction in maximum stress for cold expansion is shown to be more efficient at low stress levels than high stress levels. It is explained that plastic deformation and compressive residual stress occurs at the critical location of open hole specimen under high stress level and thus the beneficent effect of cold expansion will be discounted.

The longitudinal stress σ_X at the smallest section for the open hole and four batches of pin interference fit specimens under remote stress of 258 and 364.4 MPa are shown for two cycles in Fig. 22. For the 258 MPa case (Fig. 22(a)), the stress amplitudes of the four batches of pin interference fit specimens are shown to be significantly reduced, but the stress amplitude remain constant as the interference fit level increases from 1.0% to 4.0%. The maximum stress is shown to slightly increase as the interference fit level increases. For the 364.4 MPa case (Fig. 22(b)), the cyclic stress for the four batches of pin interference fit specimens show similar results to the 258 MPa case.

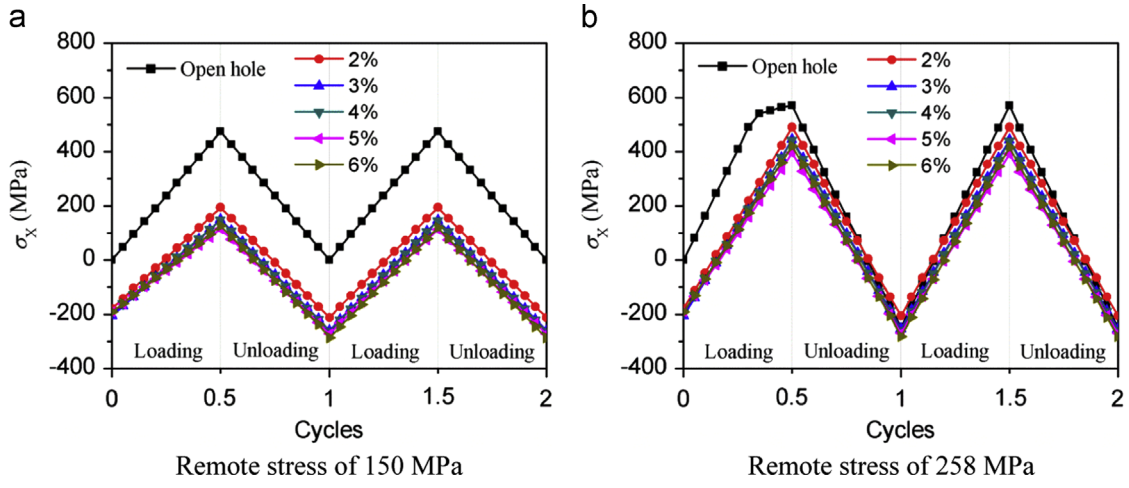

Fig. 21. Longitudinal stress σ_X at the entrance edge for the open hole and cold expanded hole specimens.

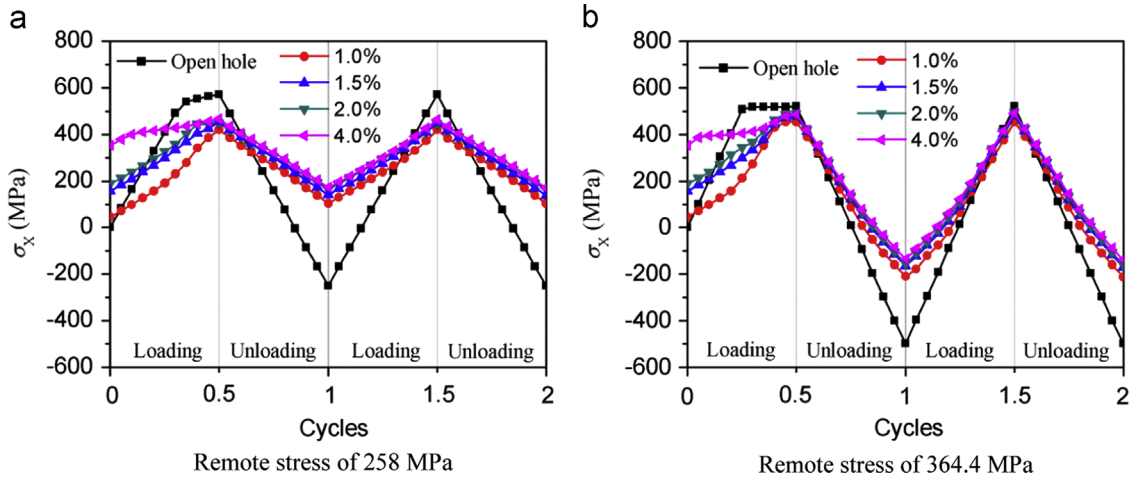

Fig. 22. Longitudinal stress σ_X at the entrance edge for the open hole and pin interference fit specimens. (a) Remote stress of 258 MPa, (b) remote stress of 364.4 MPa.

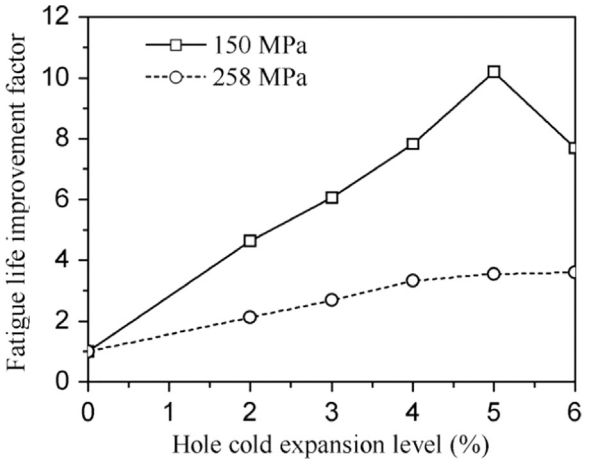

Fig. 23. Predicted LIF versus hole cold expansion level.

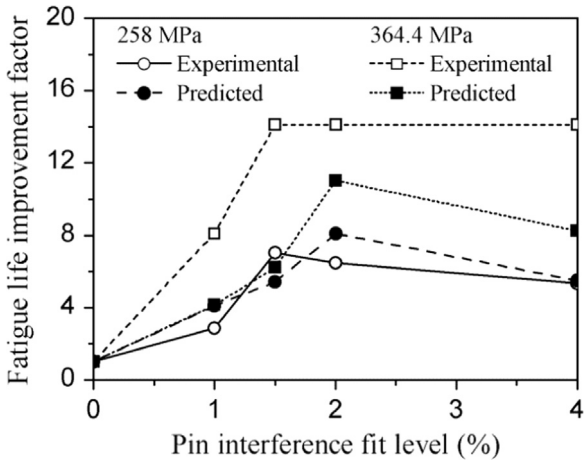

Fig. 24. Comparison of experimental and predicted LIF versus interference fit level.

5.2.4. Effect of the cold expansion and interference fit on fatigue life

A fatigue life improvement factor LIF (LIF=$N_F/N_{F,open}$=fatigue life of cold expanded or interference fit specimen/fatigue life of open hole) is used to describe the efficiency of fatigue life improvement.

Fig. 23 shows the predicted LIF versus cold expansion level (ranging from 2% to 6%) under remote stress of 150 and 258 MPa, respectively. For the 150 MPa case, the LIF is shown to increase as the cold expansion level increases from 2% to 5%, and to decrease from 5% to 6%. For the 258 MPa case, the LIF is shown to increase as the cold expansion level increases from 2% to 5%, but there is little additional improvement shown from 5% to 6%. The trend of fatigue life improvement is shown to be in general agreement with the analysis of cyclic stress. Moreover, the LIF for the 150 MPa case is shown significantly greater than the 258 MPa case. It can also be concluded that 5% is the best value of cold expansion for the studied specimen.

Fig. 24 shows the comparison of experimental and predicted LIF versus interference fit level (ranging from 1% to 4%). The predicted LIF is shown to increase as the interference fit level increases from 1% to 2%, and to decrease from 2% to 4%. The predicted results show agreeing well with the experimental results and the analysis of cyclic stress. Since the predicted fatigue lives are determined by the stress amplitude, mean hydrostatic stress and maximum von Mises stress, the trend of LIF does not fully agree with the trend of cyclic stress analysis.

6. Conclusions

The fatigue damage evolution at holes in plates treated by cold expansion or with interference fit pins is simulated by the continuum damage mechanics approach combined with the finite element method. The damage-coupled Chaboche plasticity constitutive model and damage evolution equations are used to model the material, which is implemented by UMAT in ABAQUS. The simulations are carried out in two main phases, the process of the hole cold expansion or pin interference fit and the subsequent fatigue damage evolution. The effects of cold expansion and interference fit on fatigue damage at holes in a plate are investigated quantitatively. Some key findings of this study are:

1. The proposed approach provides an insight into the fatigue damage evolution and associated material degradation of the cold expanded and pin interference fit fastener holes. The predicted fatigue lives and crack nucleation locations are in good agreement with the experimental results, the performance of proposed approach shows superior results to the critical-plane SWT method.
2. The beneficial effect of cold expansion and interference fit on the fatigue life improvement of fastener holes is not only due to the reduction of maximum stress or stress amplitude, but also due to the change in the fatigue damage evolution at the critical location.

3. The effect of hole cold expansion on fatigue life improvement is shown to be more efficient at low stress levels than that at high stress levels. The fatigue life improvement is shown to increase as the cold expansion level increases from 2% to 5%, but there is little additional improvement from 5% to 6%. The best cold expansion level for the studied specimens is predicted to be 5%.
4. The fatigue life improvement for the interference fit specimen is shown to increase as the interference fit level increases from 1% to 2%, and to decreases from 2% to 4%. The best interference fit level for the studied specimens is predicted to be 2%. The predicted results agree well with the experimental results.

References

[1] Burlat M, Julien D, Levesque M, Bui-Quoc T, Bernard M. Effect of local cold working on the fatigue life of 7475-T7351 aluminium alloy hole specimens. Eng Fract Mech 2008;75:2042–61.
[2] Chakherlou TN, Mirzajanzadeh M, Abazadeh B, Saeedi K. An investigation about interference fit effect on improving fatigue life of a holed single plate in joints. Eur J Mech A-Solid 2010;29:675–82.
[3] McNeill WA, Heston AW. Cold working fastener hole-theoretical analysis, methods of cold working, experimental results. In: Proceedings of the ASM conference on residual stresses in design, process and materials selection, Cincinnati, OH, USA; 1987. p. 193–203.
[4] Chakherlou TN, Vogwellb J. The effect of cold expansion on improving the fatigue life of fastener holes. Eng Fail Anal 2003;10:13–24.
[5] De Matos PFP, PMGP Moreira, Camanho PP, De Castro PMST. Numerical simulation of cold working of rivet holes. Finite Elem Anal Des 2005;41:989–1007.
[6] De Matos PFP, PMGP Moreira, Pina JCP, Dias AM, De Castro PMST. Residual stress effect on fatigue striation spacing in a cold-worked rivet hole. Theor Appl Fract Mech 2004;42:139–48.
[7] Lacarac V, Smith DJ, Pavier MJ, Priest M. Fatigue crack growth from plain and cold expanded holes in aluminium alloys. Int J Fatigue 2000;22:189–203.
[8] Pasta S. Fatigue crack propagation from a cold-worked hole. Eng Fract Mech 2007;74:1525–38.
[9] Crews John JH. Analytical and experimental investigation of fatigue in a sheet specimen with an interference-fit bolt. Hampton: NASA Langley Research Center; 1975. p. VA23665.
[10] Iyer K, Rubin CA, Hahn GT. Influence of interference and clamping on fretting fatigue in single rivet-row lap joints. J Tribol 2001;123:686–98.
[11] Chakherlou TN, Mirzajanzadeh M, Vogwell J. Experimental and numerical investigations into the effect of an interference fit on the fatigue life of double shear lap joints. Eng Fail Anal 2009;16:2066–80.
[12] Finney JM. Cold expansion and interference for extending the fatigue life of multi-layer metal joints. Research report 17. Australia: Defence Science and Technology Organisation. Aeronautical Research Laboratories; 1993.
[13] Sundarraj N, Dattaguru B, Ramamurthy TS. Analysis of a double shear lap joint with interference pin fit. Comput Struct 1995;55:357–63.
[14] Chakherlou TN, Abazadeh B. Estimation of fatigue life for plates including pre-treated fastener holes using different multiaxial fatigue criteria. Int J Fatigue 2011;33:343–53.
[15] Abazadeh B, Chakherlou TN, Farrahi GH, Alderliesten RC. Fatigue life estimation of bolt clamped and interference fitted-bolt clamped double shear lap joints using multiaxial fatigue criteria. Mater Des 2013;43:327–36.
[16] Glinka G, Shen G, Plumtree A. A multiaxial fatigue strain energy density parameter related to the critical plane. Fatigue Fract Eng Mater Struct 1995;18:37–46.
[17] Smith RN, Watson P, Topper TH. A stress–strain function for the fatigue of metal. J Mater 1970;5:767–78.
[18] Fatemi A, Socie DF. A critical plane approach to multiaxial fatigue damage including out-of-phase loading. Fatigue Fract Eng Mater Struct 1988;11:149–65.
[19] De Matos PFP, McEvily AJ, PMGP Moreira, De Castro PMST. Analysis of the effect of cold-working of rivet holes on the fatigue life of an aluminum alloy. Int J Fatigue 2007;29:575–86.
[20] Kachanov LM. On the creep fracture time. . Izvestiya Akademii: Nauk USSR Otd. Tech.; 1958. p. 26–31 (in Russian).
[21] Kachanov LM. Introduction to continuum damage mechanics. Boston. Dordrecht: Martinus Nijhoff Publisher; 1986.
[22] Lemaitre J. A course on damage mechanics. New York: Springer; 1992.
[23] Lemaitre J, Chaboche JL. Mechanics of solid materials. Cambridge: Cambridge University Press; 1990.
[24] Kang GZ, Liu YJ, Ding J, Gao Q. Uniaxial ratcheting and fatigue failure of tempered 42CrMo steel: damage evolution and damage-coupled visco-plastic constitutive model. J Plast 2009;25:838–60.
[25] Zhang T, McHugh PE, Leen SB. Finite element implementation of multiaxial continuum damage mechanics for plain and fretting fatigue. Int J Fatigue 2012;44:260–72.
[26] Shen F, Hu W, Meng Q. A damage mechanics approach to fretting fatigue life prediction with consideration of elasto-plastic damage model and wear. Tribol Int 2015;82:176–90.
[27] Lemaitre J, Rodrigue D. Engineering damage mechanics: ductile, creep, fatigue and brittle failures. Berlin: Springer; 2005.
[28] Chakherlou TN, Aghdam AB. An experimental investigation on the effect of short time exposure to elevated temperature on fatigue life of cold expanded fastener holes. Mater Des 2008;29:1504–11.
[29] Mirzajanzadeh M, Chakherlou TN, Vogwell J. The effect of interference-fit on fretting fatigue crack initiation and ΔK of a single pinned plate in 7075 Al-alloy. Eng Fract Mech 2011;78:1233–46.
[30] Chaboche JL. On some modifications of kinematic hardening to improve the description of ratcheting effects. J Plast 1991;7:661–78.
[31] Lemaitre J. A continuous damage mechanics model for ductile fracture. J Eng Mater Technol 1985;107:83–9.
[32] Sines G. Behavior of metals under complex static and alternating stress. In: Metal fatigue. New York: McGraw-hill; 1959.
[33] Military Handbook-MIL-HDBK-5H: metallic materials and elements for aerospace vehicle structures (Knovel interactive ed.). US Department of Defense; 1998.
[34] Dowling NE. Mechanical behavior of materials: engineering methods for deformation, fracture, and fatigue. Upper Saddle River, NJ, USA: Prentice hall; 1993.
[35] Wang YY, Yao WX. Evaluation and comparison of several multiaxial fatigue criteria. Int J Fatigue 2004;26:17–25.